bioRxiv preprint doi: https://doi.org/10.1101/2020.06.21.163931; this version posted June 22, 2020. The copyright holder for this preprint (which was not certified by peer review) is the author/funder. All rights reserved. No reuse allowed without permission.

Universal Features of Epidemic Models Under Social Distancing Guidelines

Mahdiar Sadeghi*[1], James M. Greene†[2], and Eduardo D. Sontag‡[1,3,4]

[1] *Department of Electrical and Computer Engineering, Northeastern University, Boston, MA, United States*
[2] *Department of Mathematics, Clarkson University, Potsdam, NY, United States*
[3] *Department of Biomedical Engineering, Northeastern University, Boston, MA, United States*
[3] *Laboratory of Systems Pharmacology, Harvard Medical School, Boston, MA, United States*

June 22, 2020

Abstract

Different epidemiological models, from the classical *SIR* system to more sophisticated ones involving population compartments for socially distanced, quarantined, infection aware, asymptomatic infected, and other individuals, share some remarkable dynamic characteristics when contact rates are subject to periodic or one-shot changes. In simple pulsed isolation policies, a linear relationship is found among optimal start time and duration for reduction of the infected peak. If a single interval social distancing starts *too early* or *too late* it will be ineffective with respect to decreasing the peak of infection. On the other hand, the nonlinearity of epidemic models leads to non-monotone behavior of the peak of infected population under periodic relaxation policies. This observation led us to hypothesize that an additional single interval social distancing at a *proper time* can significantly decrease the infected peak of periodic policies, and we verified this improvement.

Keywords— COVID-19, epidemic models, nonpharmaceutical interventions, optimal timing for lock-down, non-linear dynamical systems. social distancing.

1 Introduction

COVID-19, the disease first identified in Wuhan, China and the cause of the 2020 pandemic, has infected over 6.2 million people worldwide, caused at least 370K deaths, and has resulted in a worldwide economic downturn [1, 2, 3]. Social distancing as a form of Nonpharmaceutical Intervention (NPI) has been enacted in many countries as a means of reducing the spread of the virus, as no viable vaccine or herd immunity currently exists [4, 5, 6]. Many countries have implemented strict quarantine, isolation, or social distancing policies early in the epidemic [7], while some countries, like Belarus [8], and Sweden [9, 10] have taken more lenient approaches. As currently the only option to reduce transmission, understanding optimal strategies for social distancing will both "flatten the curve" and hopefully ease the economic burden experienced due to prolonged economic stagnation [11, 12, 13, 14, 15, 16]. The goal of this manuscript is to thus investigate the response of the disease to different time-varying social distancing strategies.

Besides the recent theoretical efforts [17, 18, 19, 20], various population models have been applied to capture the spread of COVID-19. These models have been used to predict the potential number of infected individuals and virus-related deaths, as well as to aid government agencies in decision making [21, 22]. Most models are variations on the classical Susceptible-Infected-Recovered (*SIR*) model [23, 24, 25] which have been modified to more closely capture characteristic features of the current pandemic. Some such extensions are listed below:

1. Expanding the *SIR* model to include additional population compartments. Such compartments may describe individuals that are placed under quarantine and/or in social isolation. Other models explicitly subdivide populations into both symptomatic and asymptomatic infected individuals [26, 27, 28, 29, 30, 31, 32, 33, 34, 35, 36, 37, 38, 39], as it is currently thought that COVID-19 is significantly spread through *asymptomatic* individuals [40, 41, 42, 43].

*mahdiar@coe.neu.edu, ORCID: 0000-0002-8696-0912
†jgreene@clarkson.edu, ORCID: 0000-0003-0954-2730
‡sontag@sontaglab.org, ORCID: 0000-0001-8020-5783

bioRxiv preprint doi: https://doi.org/10.1101/2020.06.21.163931; this version posted June 22, 2020. The copyright holder for this preprint (which was not certified by peer review) is the author/funder. All rights reserved. No reuse allowed without permission.

2. Modeling the effects of social distancing for an infection aware population. This can be done by changing the contact rates between the compartments, or by modeling the behavior of a population that alters its social interactions because of observed infections or deaths [44, 45]. The latter technique has recently been applied to COVID-19 [46, 47].
3. Sub-dividing populations into regions, each described by *local* parameters. Such regions may be cities, neighborhoods, or communities [48]. This framework allows modelers to capture the virus spread and population mobility geographically [49, 50, 51, 52, 53]. These models have been recently used to understand the spread of COVID-19 in China [54], Italy [55], Belgium [56], and India [57, 58].

We begin by investigating one-shot social distancing policies on the overall peak reduction in the infected population. A number of *SIR* model variants are simulated, as well as related epidemic models that have been recently proposed to describe the transmission of COVID-19. We numerically discover a near linear optimal trade-off between the social distancing start time and duration, which seems to be ubiquitous among all models considered. This behavior can explained by analytical considerations, at least for the *SIR* model.

Shortening the period of time that populations are socially distanced is economically advantageous [59, 60, 61, 62, 63]. The main objective of this study is to reduce the disease burden (here measured as the peak of the infected population) while simultaneously minimizing the length of time the population is socially distanced. The timing of one-shot pulses is analyzed, but other policies may be preferred economically. For example, we also consider periodically relaxing social distancing mandates, which allow for scheduled economic activity. However, we find that such policies lead to a none-monotone dependence of the infected peak as a function of the period time [64, 26]. Of course, such strategies are not preferable if they do not significantly result in the reduction of the infected peak.

Our simulations and analysis suggest that the peak of infected population under periodic relaxation or mild social distancing policies can be significantly reduced (by $30-50\%$), if they are combined with a strict single pulse of social distancing at a *proper time*. On the other hand, if a one-shot social distancing pulse begins *too early* (e.g. India [65, 66]), or *too late* it will not be an effective measure for inhibiting disease response.

2 Modeling

Deterministic population models are commonly used to model the spread of an epidemic like COVID-19 [24, 23, 26]. Although some assumptions (such as population homogeneity) are not precisely accurate, such frameworks still provide invaluable insight in predicting the spread of the disease, and can be utilized to inform policy decisions in the presence of a pandemic.

We note that in models described by Ordinary Differential Equations (ODE), infections may be eradicated *only asymptotically*; that is, at any finite time, the proportion of infected individuals will be non-zero. Of course, physically this is unrealistic, and if the proportion of individuals affected is less than the proportion of a single person, the disease should be deemed eradicated. We note that this can be implemented via a threshold for the infected compartment (e.g. a proportion of 10^{-7}), where the disease is considered eradicated once the infected compartment drops below this threshold. Alternatively, one may use corresponding stochastic models that may (with non-zero probability) reach zero in finite time.

2.1 Review of *SIR* model

The standard *SIR* model [23] takes the form:

$$\dot{S} = -\beta SI, \tag{1a}$$

$$\dot{I} = \beta SI - \gamma I, \tag{1b}$$

$$\dot{R} = \gamma I. \tag{1c}$$

Here β is the transmission rate between the susceptible S and infected I individuals in a well-mixed population, and γ is the rate of recovery into the recovered (removed) R compartment. The *SIR* model can be used as an approximation to COVID-19 dynamics if immunity is long-lasting, which seems appropriate given time scales of the distancing policies considered here (less than one year, see below). Note that deceased and recovered individuals are combined into a single removed compartment R. The initial conditions are fixed as $(S(0), I(0), 0)$ with a small initial value for the infected compartment $I(0)$, and

$$S(0) + I(0) = 1. \tag{2}$$

That is, we have normalized so that all compartments denote percentage of population, and not raw population numbers. We may translate directly to raw population numbers by multiplying fractions by the initial susceptible population.

In this work, we use the peak of the infected population (measured as a fraction of the total population) as our primary measure of epidemic severity; the larger the peak, the worse the response. The peak of the

bioRxiv preprint doi: https://doi.org/10.1101/2020.06.21.163931; this version posted June 22, 2020. The copyright holder for this preprint (which was not certified by peer review) is the author/funder. All rights reserved. No reuse allowed without permission.

infected compartment (I_p) can be derived analytically as a function of the initial conditions. We have included the derivation of the following formulas in Appendix A.1 for convenience of the reader. Denoting the peak of I by I_p, and the corresponding susceptible population by S_p, we compute that if $S(0) > R_0^{-1}$,

$$S_p = \gamma/\beta = R_0^{-1}, \tag{3a}$$

$$I_p = I(0) + S(0) - R_0^{-1}(1 + \ln(S(0)R_0)). \tag{3b}$$

Here

$$R_0 := \frac{\beta}{\gamma}. \tag{4}$$

denotes the basic reproduction number of the *SIR* model. Note that the maximum of the infected compartment is only a function of the basic reproduction number R_0.

2.2 Single interval social distancing

Social distancing is currently being implemented via a variety of different techniques. For example, in many locations local and federal governments are issuing rules related to quarantine and isolation, as well as regulations for wearing masks and avoiding non-essential interactions to reduce contact rates [67]. In the *SIR* model discussed in Section 2.1, social distancing may be mathematically modeled by temporarily reducing the transmission rate of the disease β. As an example, consider a single interval of social distancing (a one-shot pulse), represented mathematically as a time-varying transmission rate $\beta(t)$ in Eq. (5). Here we assume that β can be effectively reduced from β_n to β_d during distancing. For a visualization, see Fig. 1. Here distancing regulations are enacted at day t_s, which corresponds to a decrease in the transmission rate $\beta_n \to \beta_d$. Regulations are implemented until day $t_s + t_d$, after which they are completely relaxed, i.e. $\beta_d \to \beta_n$. Note that for other models, distancing may be implemented differently. For example, in an infection-aware community, viral transmission may be reduced as the number of confirmed cases increases during an epidemic [46], hence yielding a feedback law governing $\beta = \beta(I)$.

$$\beta(t) = \begin{cases} \beta_n, & 0 < t_s \\ \beta_d, & t_s \le t < t_s + t_d \\ \beta_n, & t_s + t_d \le t \end{cases}. \tag{5}$$

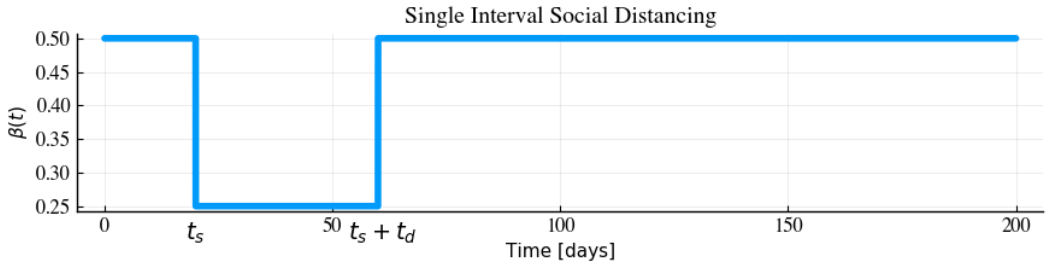

Figure 1: Single interval social distancing during an epidemic for the *SIR* model. Here social distancing starts at day $t_s = 20$, and lasts for $t_d = 40$ days, after which regulations are completely relaxed.

We begin by considering how the start time t_s and duration t_d affect the peak of the infected compartment. Note that prolonged distancing cannot be enacted without severe economical/sociological consequences, so that the timing of an *interval* of distancing is of great interest. A rigorous analysis has been performed in [68] to find the optimal schedule of distancing based on the *SIR* model and cost function that minimizes a combination of the total number of deaths and the peak of the infected compartment. Indeed, the authors in [68] find a distancing policy of the form (5) as optimal, which motivates us to investigate the precise switching times t_s and t_d. That is, we are interested in understanding *when* social distancing should be implemented for a specific distancing period. In the following we will study this problem for a subset of recently proposed models that have been introduced to understand the spread of COVID-19.

3 Results

In this section, we investigate how the peak of infected population is affected by the start time t_s for a finite duration of social distancing t_d (see Fig. 1, which represents a simple model of single interval social distancing as one-shot pulse input). We begin with the *SIR* model and observe a linear trade off between the start time and duration of social distancing. We note a distinctive "V" shaped pattern in the heat maps/contour plots, and

bioRxiv preprint doi: https://doi.org/10.1101/2020.06.21.163931; this version posted June 22, 2020. The copyright holder for this preprint (which was not certified by peer review) is the author/funder. All rights reserved. No reuse allowed without permission.

analyze this geometry mathematically. Then, we perform similar numerical simulations for other related epidemic models that have been recently proposed for describing COVID-19: *SAIR* model, *fSIR* [46], 6 Compartment *SIR* model [26], *SIQR* model [37], and *SIDARTHE* model [36]. We find that the "V" shaped pattern is consistent among all of these models, and we believe it is a universal feature in epidemic models. Lastly, we investigate the relation between "mild" social distancing and periodic relaxations that has been recently proposed by [69, 64]; our goal is to understand their limitations. We also show that a well-timed one-shot social distancing pulse can significantly reduce the infected peak, when applied in conjunction with periodic relaxation or mild social distancing strategies.

3.1 Single-pulse response

Fig. 2 represents the peak infected population in response to a single interval of social distancing for the *SIR* model (see Fig. 1). The dashed vertical line in Fig. 2a indicates the at which the infected peak under no distancing mandates would peak; we call this the "virtual peak". Note that implementing social distancing after the vertical line (*too late* start time t_s) has no effect on infected peak reduction. In general, we observe that there are schedules such that one-shot pulses effectively reduce the infected peak up to 50% of the virtual peak. Specifically, from the left side of the dashed vertical line, we see that social distancing can be effective if it is implemented early enough.

We denote the combination of diagonal and vertical sections of the contours in Fig. 2b as a characteristic "V" shaped pattern. Intuitively, we expect a vertical line as the boundary between the blue and white area in Fig. 2a, because implementing *too late* means that distancing policies will have little effect on reducing the spread of the disease; there are already too many infected individuals. Indeed, it is clear that as we decrease β (enact social distancing), the peak of infected population decreases, *if social distancing is enacted quickly enough.* Similarly, any social distancing policy initiated after the virtual peak would be ineffective in decreasing the peak (see Section 3.2).

However, we note a large transition region in start times t_s, *before* the non-distanced peak actually occurs; that is, distancing must be implemented before the peak of infectivity if we are to significantly inhibit the disease burden. This is non-intuitive, and it is important for policy-makers to understand this *gap* during which one-shot pulses are sensitive to the start time t_s. This can be explained by sensitivity of the infected peak to start time, with details provided in Section 3.2. The infected peak is very sensitive to start times in a narrow band, due primarily to sensitivity of the integral curves of the SIR model in a region of (S,I) phase-space. In the provided simulations (Fig. 2), the time scales are on the orders of days, but in general depend on specific parameter values.

The diagonal dashed line in Fig. 2b represents an almost linear trade-off between the start and the duration of the social distancing. We can understand this theoretically, and show that the slope of this line is approximately dependent only on the ratio between the non-distanced and distanced transitions rates (β_n and β_d, respectively):

$$-\frac{\beta_n}{\beta_d} \tag{6}$$

For example, the slope of the diagonal line in Fig. 2b is approximately -2, with $\beta_d = 0.25$ and $\beta_n = 0.5$.

We argue as follows the: consider the linear approximation for the infected peak (42), derived in Section A.3. For convenience, we provide the formula below:

$$I(t) \approx I(0) \exp\left((\beta - \gamma)t\right). \tag{7}$$

Hence, if t_p denotes the time of the peak infected population, we have

$$I_p \approx I(0) \exp\left((\beta - \gamma)t_p\right). \tag{8}$$

To understand the dynamics, intuitively one can utilize the above formula from $t = 0$ to $t = t_s$ with no social distancing enacted, and one-shot pulse with duration of t_d (i.e. from time $t = t_s$ to $t = t_s + t_d$). Note that the two formulas are connected via their initial conditions, which are $I(0)$ and $I(t_s)$, respectively. Hence, the infected compartment at time $t = t_s + t_d$ can be approximated as:

$$I(t = t_s + t_d) \approx I(0) \exp\left((\beta_n - \gamma)t_s + (\beta_d - \gamma)t_d\right). \tag{9}$$

If the infected compartment reaches its fixed maximum value at time $t_p = t_s + t_d$, then equation (9) implies that t_s and t_d are related by

$$(\beta_n - \gamma)t_s + (\beta_d - \gamma)t_d = \tilde{C}, \tag{10}$$

for a constant $\tilde{C}$. Since $t_s + t_d = t_p$, the above becomes

$$\beta_n t_s + \beta_d t_d = C, \tag{11}$$

where $C := \tilde{C} - \gamma t_p$. Hence the contours of constants $I_{\max}$ in Fig. 2b can be approximated by parallel lines, each with the slope computed in (6).

bioRxiv preprint doi: https://doi.org/10.1101/2020.06.21.163931; this version posted June 22, 2020. The copyright holder for this preprint (which was not certified by peer review) is the author/funder. All rights reserved. No reuse allowed without permission.

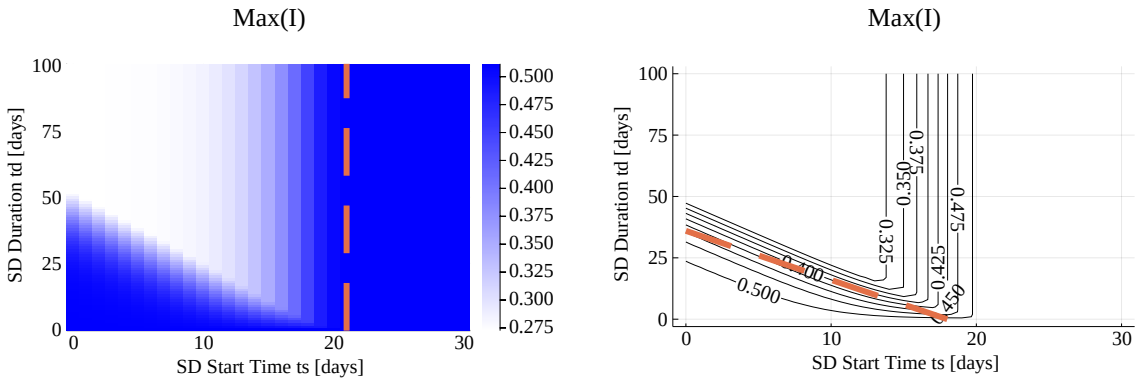

(a) Heat map of peak of infected peak.

(b) Contour plot of peak of infected peak.

Figure 2: Infected peak under single interval social distancing (SD) policy that starts from $t = t_s$ until $t = t_s + t_d$ for *SIR* model.

By observing the contours of Fig. 2b, we see a similar parallel structure. The diagonal dashed line represents the slope computed by (6), which appears to agree with the contour lines.

The blue region at the bottom left side of the Fig. 2a represents the social distancing policies with short duration that start *too early*. The higher infected peak indicates that the peak of the infected compartment occurs after the social distancing relaxation. Although such policies delay the infected peak and provide more time for discovery of new testing and treatment methods, they are not effective in flattening the curve and reducing the infected peak. We believe the the current situation in India [65], is an example of ineffective single interval social distancing.

3.2 A theoretical explanation for the phase transition observed in Figure 2a

Figure 2a exhibits a remarkable feature: there is a phase transition from effective (white) to ineffective (blue) policies, depending on the starting time of distancing policies. We asked if this fact, observed from simulations, can be understood theoretically. In other words, can we estimate the rather narrow region where the transition occurs?

We answer this question as follows. We consider the *SIR* model, where social distancing is initiated at time t_s. Note that we are analyzing the behavior of the model with respect to the horizontal axis in Figure 2; in this Section we thus ignore the duration of distancing (t_d) and hence assume distancing remains in effect until the end of the simulation. Here we give a characterization of peak of the infected population as a function of t_s.

Fix an *SIR* model with time-varying $\beta(t)$, such that

$$\beta(t) = \begin{cases} \beta_n, & 0 \le t \le t_s \\ \beta_d, & t_s < t \le t_f \end{cases}. \tag{12}$$

We assume that $\beta_n > \beta_d$, so that distancing has the effect of reducing the transmission rate of the disease. Here t_f is the entire period under consideration. Our goal is to understand the peak of the infected population, I_p, as a function of the switching time t_s.

Note that by changing β_n to β_d we have effectively reduced the basic reproduction number R_0:

$$R_0(\beta) = \frac{\beta}{\gamma} \tag{13}$$

From equation (3a), we see that such a switch then increases the value S_p where the global maximum value of I occurs:

$$S_p(\beta) = \frac{1}{R_0(\beta)}. \tag{14}$$

This then allows us to compute the value of I_p as a function of the state $(S(t_s), I(t_s))$, where t_s is the time at which social distancing is implemented. We first assume that both β_n and β_d are such that

$$R_0(\beta_n), R_0(\beta_d) > 1. \tag{15}$$

The above then implies that the infected population may increase in both the normal and distanced environments, if the susceptible population at the distancing time t_s is large enough (see (19) below). Note that this matches

bioRxiv preprint doi: https://doi.org/10.1101/2020.06.21.163931; this version posted June 22, 2020. The copyright holder for this preprint (which was not certified by peer review) is the author/funder. All rights reserved. No reuse allowed without permission.

the parameter values utilized in Figure 2, where

$$R_0(\beta_n) = 5.56 \tag{16}$$
$$R_0(\beta_d) = 2.78. \tag{17}$$

Since R_0 increases as a function of β, equation (14) implies that

$$S_p(\beta_n) < S_p(\beta_d) \tag{18}$$

Assuming (15), we are able to compute the maximum of the infected population as a function of the susceptible population at the time t_s:

$$I_p = \begin{cases} I(t_s) + S(t_s) - \frac{1}{R_0(\beta_d)}(1 + \log(S(t_s)R_0(\beta_d))), & S_p(\beta_d) \leq S(t_s) \leq 1 \\ I(t_s), & S_p(\beta_n) \leq S(t_s) \leq S_p(\beta_d) \\ S(0) + I(0) - \frac{1}{R_0(\beta_n)}(1 + \log(S(0)R_0(\beta_n))), & 0 \leq S(t_s) < S_p(\beta_n) \end{cases} \tag{19}$$

Equation (19) can be understood as follows. Recall that $S(0) \approx 1$ and that S is decreasing. Hence an early time t_s corresponds to $S(t_s)$ close to 1, while waiting longer decreases the value $S(t_s)$. Hence left-to-right in Figure 2 corresponds to top-to-bottom in equations (19).

The first case occurs if t_s is less than the time at which the peak value of the infective state would have been attained, if one had imposed social distancing from time zero. Note this peak always occurs, as a function of state S, *before* the non-distanced peak by (18). Specifically, I was increasing for $t \in [0, t_s]$ and at t_s satisfies

$$\lim_{t \to t_s^-} \frac{dI}{dt}(t) \geq 0 \tag{20}$$
$$\lim_{t \to t_s^+} \frac{dI}{dt}(t) \geq 0 \tag{21}$$

Thus, I is increasing at t_s, and as $\beta(t) \equiv \beta_d$ for $t > t_s$, the maximum of I (for all $t \in [0, t_f]$) occurs at the peak of the distanced dynamics, which is given by (41c), with new initial conditions $(S(t_s), I(t_s))$ and $R_0 = R_0(\beta_d)$. This is precisely the first formula in (19).

If time t_s is large enough so that $S_p(\beta_n) \leq S(t_s) \leq S_p(\beta_d)$, then $I(t)$ must satisfy

$$\lim_{t \to t_s^-} \frac{dI}{dt}(t) \geq 0 \tag{22}$$
$$\lim_{t \to t_s^+} \frac{dI}{dt}(t) \leq 0. \tag{23}$$

Since I was increasing for $0 \leq t \leq t_s$, the maximum of I occurs at $t = t_s$, and is the second formula in (41c).

Lastly, if t_s is long enough so that $S(t_s) < S_p(\beta_n)$, then

$$\lim_{t \to t_s^-} \frac{dI}{dt}(t) \leq 0 \tag{24}$$
$$\lim_{t \to t_s^+} \frac{dI}{dt}(t) \leq 0. \tag{25}$$

Thus, the peak of the infected compartment occurred at an earlier time, before distancing was enacted, with $\beta = \beta_n$. This peak value is given precisely by (41c), with $\beta = \beta_n$, since the overall peak value is given by the peak value of the non-distanced dynamics; this corresponds to the third formula in (41c). For a visualization of all three cases, see Figure 3.

Formula (19) allows us to estimate the differential sensitivity of I_p with respect to t_s. First note this is approximately proportional to the differential sensitivity of I_p with respect to $I(t_s)$, since (assuming $S(0) \approx 1$ and that S is relatively constant on $[0, t_s]$):

$$I(t_s) \approx I(0)e^{(\beta_n - \gamma)t_s}, \tag{26}$$

or

$$\log(I(t_s)) \approx \log(I(0)) + (\beta_n - \gamma)t_s \tag{27}$$

That is, the two differential sensitivities (I_p with respect t_s, and I_p with respect to $I(t_s)$) differ by a constant factor $\beta_n - \gamma$. In the remainder, we compute the differential sensitivity of I_p with respect to $I(t_s)$ as a proxy for the true sensitivity of I_p with respect to t_s (the quantity of interest from Figure 2).

We first note that I_p is a function of $I(t_s)$ only if the latter's range is restricted to include regions where $I(t_s)$ is invertible (with respect to t_s). Since $I(t_s)$ has a relative maximum at distancing time t_s such that $S(t_s) = S_p(\beta_n)$, it is clear that the domain of I_p must be restricted into two regions: $I(t_s)$ with $S(t_s) \in [S_p(\beta_n), 1]$ (where $I(t_s)$

bioRxiv preprint doi: https://doi.org/10.1101/2020.06.21.163931; this version posted June 22, 2020. The copyright holder for this preprint (which was not certified by peer review) is the author/funder. All rights reserved. No reuse allowed without permission.

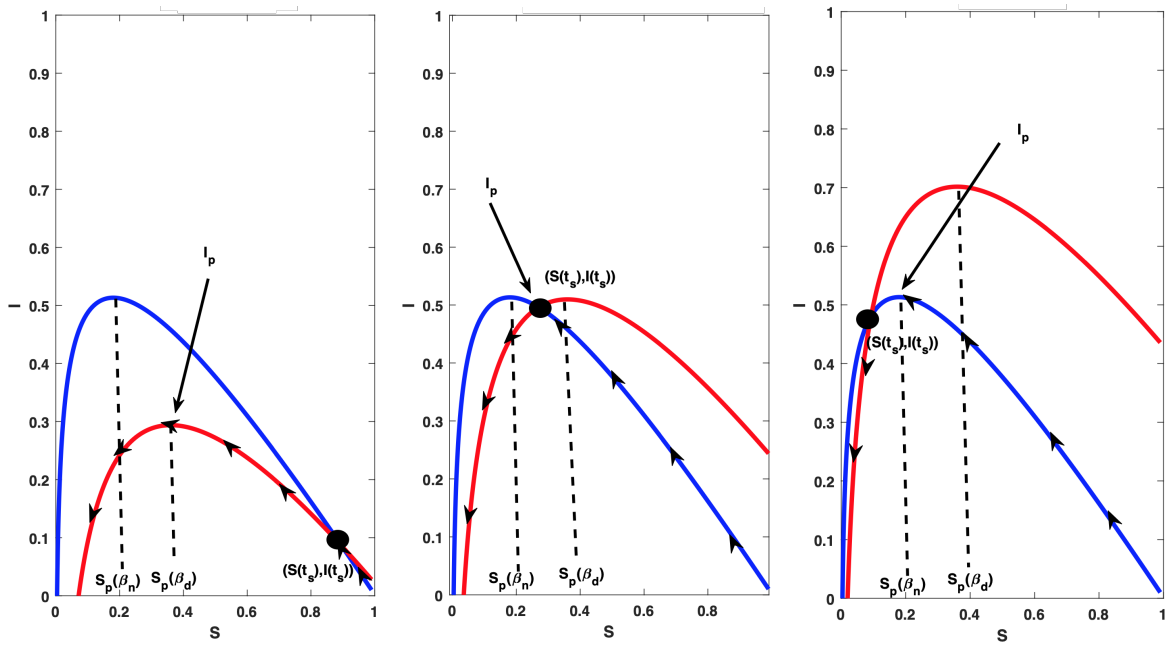

(a) $S_p(\beta_d) < S(t_s)$. (b) $S_p(\beta_n) < S(t_s) < S_p(\beta_d)$. (c) $S(t_s) < S_p(\beta_n)$.

Figure 3: Integral curves defined by changing β (see equation (12). The blue curve corresponds to $\beta = \beta_n$ (non-distanced), and the red corresponds to $\beta = \beta_d$ (socially distanced). The time t_s denotes the time when social distancing is enacted. All cases assume $S(0) \approx 1$. The three figures (left-to-right) denote the three different formulas in equation (19) for I_p (top-to-bottom).

is non-decreasing) and $I(t_s)$ with $S(t_s) \in [0, S_p(\beta_n))$ (where $I(t_s)$ is decreasing). With the above understanding as to an appropriate domain, we compute the differential sensitivity of I_p with respect to $I(t_s)$:

$$\frac{d \log I_p}{d \log I(t_s)} = \frac{I(t_s)}{I_p} \cdot \frac{dI_p}{dI(t_s)}. \tag{28}$$

Equation (19) then allows us to immediately compute the sensitivity if $I(t_s)$ is such that $S(t_s) \in [0, S_p(\beta_d))$:

$$\frac{d \log I_p}{d \log I(t_s)} = \begin{cases} 1, & S_p(\beta_n) \le S(t_s) \le S_p(\beta_d) \\ 0, & 0 \le S(t_s) < S_p(\beta_n). \end{cases} \tag{29}$$

Note that the above regions correspond to Figures 3b- 3c, and is obtained by differentiating the second and third formulas in (19). In words, (29) says that the differential sensitivity is relatively large and constant for t_s such that $S_p(\beta_n) \le S(t_s) \le S_p(\beta_d)$, and then drops to 0 for larger t_s (recall that $S(t_s)$ decreases as a function of t_s). Thus the social distancing start time should have no effect on I_p if $S(t_s) < S_p(\beta_n)$, whereas there is a band of social distancing start times where I_p increases rapidly. Note for the parameter values utilized in Figure 2, we compute

$$S_p(\beta_n) = 0.18 \tag{30}$$
$$S_p(\beta_d) = 0.36, \tag{31}$$

and simulating we obtain the corresponding critical start time region (where $S(t_s) = S_p(\beta_d), S_p(\beta_n)$) as

$$t_s \in [17.72, 21.35] \text{ days}. \tag{32}$$

This is in close agreement with the region observed in Figure 2, and hence describes the vertical transition band numerically computed.

Analyzing the sensitivity at earlier start times (t_s such that $S(t_s) \in (S_p(\beta_d), 1)$) is more challenging using equation (19), since it requires taking a derivative of $S(t_s)$ with respect to $I(t_s)$. We note that we expect the sensitivity to be small for sufficiently early distancing times t_s, since we observe only slight variation in I_p from Figure 2 at small t_s (and large t_d, as we are not relaxing social distancing in this analysis). *Hence we conjecture that the sensitivity is largest exactly in the band given by* (32).

Numerically we compute the differential sensitivity of I_p for the first two regions given in (19) (t_s such that $S(t_s) \in [S_p(\beta_n), 1]$); see the black curve in Figure 4. The two regions plotted correspond to the times t_s where $I(t_s)$ is increasing. Note the approximate constant sensitivity of 1, as predicted by the first expression in (29),

bioRxiv preprint doi: https://doi.org/10.1101/2020.06.21.163931; this version posted June 22, 2020. The copyright holder for this preprint (which was not certified by peer review) is the author/funder. All rights reserved. No reuse allowed without permission.

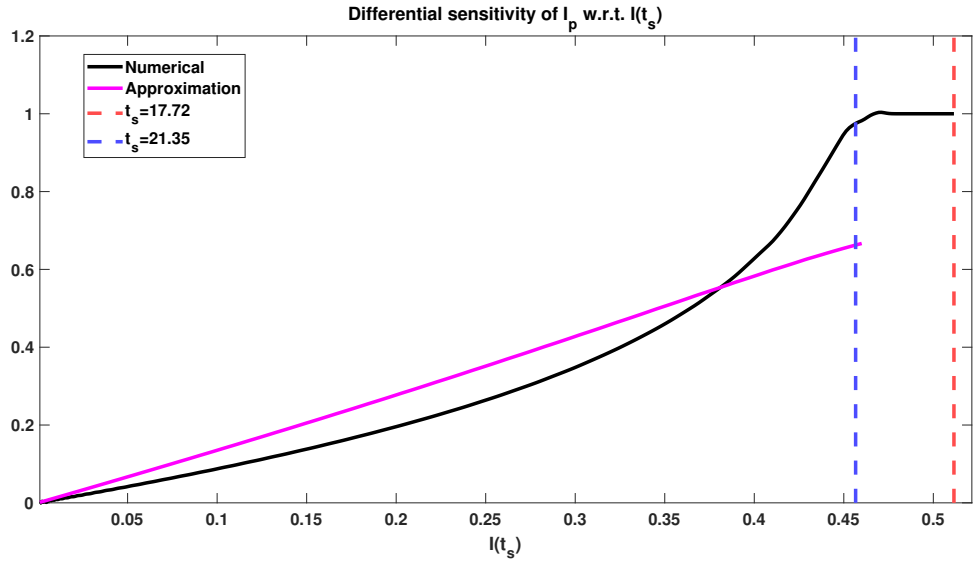

Figure 4: Differential sensitivity of I_p with respect to $I(t_s)$. Numerical approximation of sensitivity is indicated by the black curve, corresponding to region where $I(t_s)$ is increasing (first two formulas in (19)). Vertical lines denote transition regions in (19). Magenta curve is approximation to sensitivity given by equation (34).

for t_s such that $S(t_s) \in (S_p(\beta_n), S_p(\beta_d))$. We further observe a small sensitivity for small $I(t_s)$ (hence small t_s), which was also expected from Figure 2. The differential sensitivity then appears to gradually increase in value, until it reaches 1 near the transition region ($S(t_s) = S_p(\beta_d)$, blue dashed vertical line). As computed in (29), the sensitivity is 0 for larger $I(t_s)$, which is not shown in Figure 4; the red vertical line indicates the region after which the sensitivity drops to 0. A small overshoot in the figure is most likely due to numerical error, as the computation requires numerical differentiation, and was pre-processed via local averaging. Hence, at least for parameter values utilized in the above, we find an interval of critical distancing start times for which the maximum of the infected population is most sensitive.

Lastly, we approximate the differential sensitivity in the initial region where $\frac{d \log I_p}{d \log I(t_s)}$ increases from 0 to 1 by making the approximation that

$$S(t_s) + I(t_s) = 1 \tag{33}$$

in (19). Note that this should be accurate for small t_s, when $R(t_s) \approx 0$, but in general will not be true for larger times. Replacing $S(t_s)$ by $1 - I(t_s)$ in the first formula of (19) and differentiating with respect to $I(t_s)$ yields the approximation

$$\frac{d \log I_p}{d \log I(t_s)} \approx \frac{1}{R_0(\beta_d)} \cdot \frac{1}{1 - I(t_s)} \cdot \frac{I(t_s)}{I_p}, \tag{34}$$

where $S_p(\beta_d) < S(t_s) < 1$. This formula is the magenta curve in Figure 4. As expected, this approximation seems to be accurate initially, but soon diverges from the correct value.

3.3 Are dynamic properties universal features of more complex models?

One may reasonably ask whether the features observed for the *SIR* model hold as well for such more complex examples. For example, is the "V shape" in Figure 2 a universal property? Surprisingly, we can answer this positively. The *SIR* model is relatively simple, and thus its properties are easier to analyze compared to complex multi-compartment systems. However, we can use simulations for thse models to investigate the universality of the phenomenon.

We now investigate several epidemic models that have been recently formulated to capture the spread of COVID-19. Each model is simulated as in Section 3.1 utilizing parameters that have been suggested by the corresponding authors as well describing the current COVID-19 pandemic (for currently available data).

SIAR is a simple variation of the *SIR* model that includes an additional compartment A for asymptomatic infected individuals. *fSIR* is an infection aware population model with the same number of compartments as the *SIR* model, and an additional assumption that contact rates between individuals will decrease by the increase of infected compartment [46]. The 6 Compartment *SIR* model is a variation of the *SIR* model that is obtained by dividing the susceptible population into two categories: socially distanced and non-distanced populations [26].

bioRxiv preprint doi: https://doi.org/10.1101/2020.06.21.163931; this version posted June 22, 2020. The copyright holder for this preprint (which was not certified by peer review) is the author/funder. All rights reserved. No reuse allowed without permission.

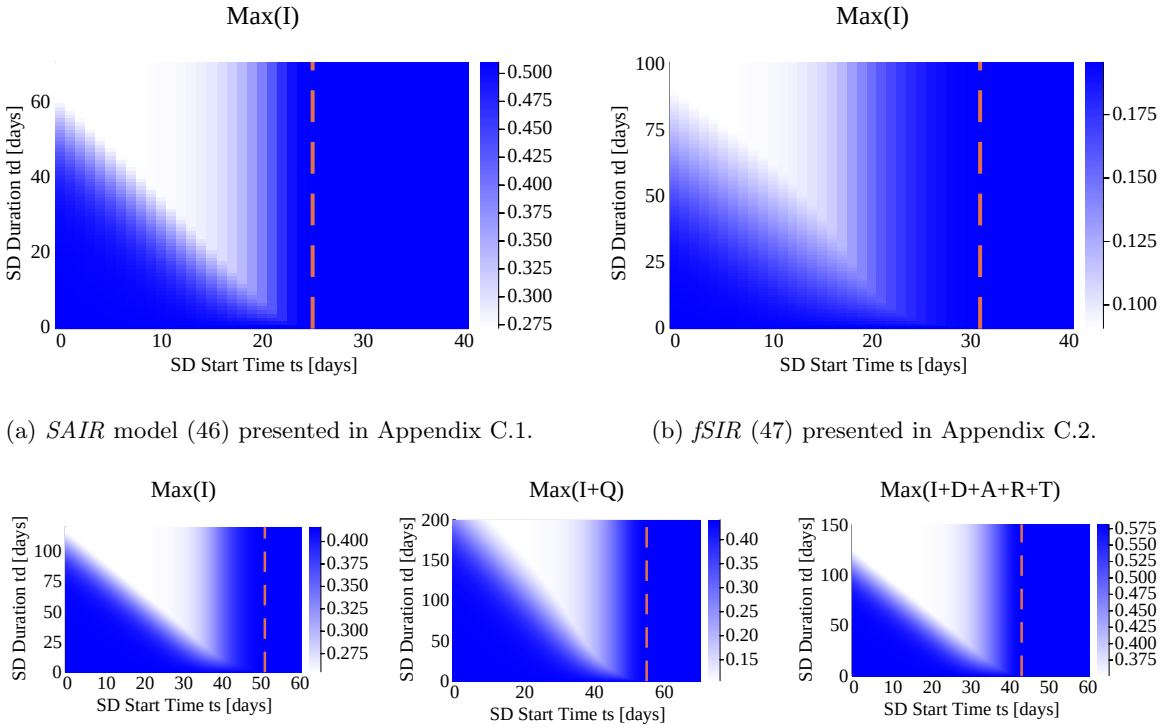

(a) *SAIR* model (46) presented in Appendix C.1.

(b) *fSIR* (47) presented in Appendix C.2.

(c) 6 Compartment *SIR* model (48) presented in Appendix C.3.

(d) *SIQR* model (49) presented in Appendix C.4.

(e) *SIDARTHE* model (50) presented in Appendix C.5.

Figure 5: Recent models proposed to capture the COVID-19 behavior show the "V" pattern. Models and their parameters are fully presented in Appendix C. The ratio between transmission rates of normal and socially distanced populations (β_n/β_d) is fixed at 2 for all models.

The *SIQR* model is also a variation of the *SIR* model that includes an additional compartment Q for the quarantined population [37], and the *SIDARTHE* model is a more complicated variation of the *SIR* model with 8 different compartments proposed by [36].

The "V" shape pattern observed in Fig. 2 seems to be consistent among these more complicated epidemic models (Fig. 5) and similar trade-offs between the start time and duration of social distancing exist.

Although the range of the infected peak is different among these models, the reduction in magnitude between the virtual peak and that under socially distancing is about 50% in every case. Also, the slope of the diagonal border between the blue (high) and white (low) regions can be approximated by the ratio between the transmission rates on normal and socially distanced populations: $-\beta_n/\beta_d = -2$.

3.4 Mild social distancing or periodic relaxation

From an economic perspective, periodic relaxation of social distancing is favorable compared to single interval strategies [69]. A policy with regular periods of distancing and relaxation can significantly delay the time of the peak of the epidemic, while still allowing limited economic activity [69, 64, 26].

Fig. 6 represents numerical simulations of the *SIR* model showing the magnitude of the infected peak under periodic relaxation with different periods T shown on horizontal axis, and the ratio of social distancing r (closed business time ratio) on the vertical axis. From Fig. 6b, it can be observed that as the period T decreases, the infected peak converges to the response corresponding to a constant $\beta(t)$ which represents the weighted average transmission rate (Appendix B). On the other hand, as the period T increases, the infected peak will be less dependent on the weighted average of the transmission rate. Observe that the infected peak is not monotonic with respect to the period T of the periodic social distancing relaxation policy, and the ratio r of distancing. In section 3.5, we argue that this behavior is due to not having a social distancing mandate at critical times (at the potential peak of the infected compartment).

This behavior has been also observed in [26, 64]. By combining results of this section and the previous section we suggest implementing periodic social distancing during an epidemic in combination with a single interval social distancing pulse at a critical time to optimally reduce the infected peak I_p.

For systems that are affine in control, fast switching policies are similar to mild social distancing with transmission rate β_m, which defined as a weighted average of $\beta(t)$ over one period (Appendix B). The limitation of such policies is that the peak of the infected population is a function of both β_n and β_d, while the peak of

bioRxiv preprint doi: https://doi.org/10.1101/2020.06.21.163931; this version posted June 22, 2020. The copyright holder for this preprint (which was not certified by peer review) is the author/funder. All rights reserved. No reuse allowed without permission.

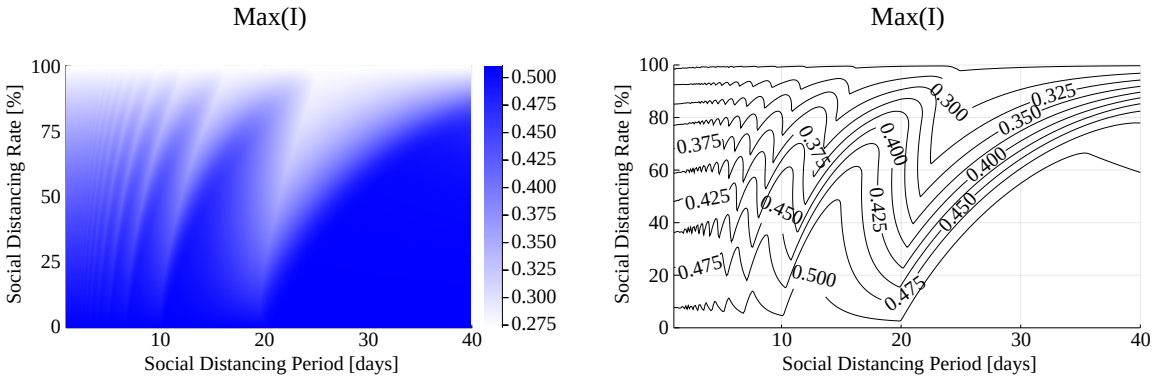

(a) Heatmap of max(I).

(b) Contours of max(I).

Figure 6: Infected peak max(I) of *SIR* model (1) for various periodic distancing relaxation of policies with different period T and ratio of social distancing r.

infected population with a single interval social distancing at a *proper time* will be only dependent on the social distancing transmission ratio β_d. The infected peak is a non-monotonic function of social distancing period T and ratio r. In what follows, we propose a combination of a single-pulse and periodic social distancing policy as an approach that allows reducing the infected peak as much as possible while having the economic benefit and a delayed peak as with a periodic policy.

3.5 Periodic relaxation combined with a single interval of social distancing

The peak of infected population depends non-monotonically on both the period T and ratio r of periodic policies. A periodic social distancing relaxation policy with a large period time T may lead to not having a social distancing mandate at the critical time of an epidemic (at the potential peak of the infected population) or it may lead to a well-timed social distancing and significantly reduce the infected peak. To address this uncertainty, we propose combining single-pulse social distancing with a periodic relaxation policy.

Fig. 7 illustrates the effect of combining a single pulse of social distancing with mild social distancing and periodic relaxation policies with different periods T for the *SIR* model. The transmission rate used as an input for the pulsed strategy is visualized in Fig. 7a. This representation is for periodic social distancing with period of one week $T = 7$, with two days relaxation and five days social distancing strategy, which means that the ratio is $r = 5/7$. The single-pulsed strategy with different start time t_s and duration t_d is simulated in combination with a mild social distancing (Fig. 7b) and periodic pulsed strategies (Figs. 7c, 7d, and 7e). By comparing the dark blue (high) and white (low) regions in Fig. 7 it can be observed that the infected peak, that is dependent on the weighted average of transmission rate over time, can be reduced by 30% percent with just one additional single-pulse social distancing at an appropriate time.

Figs. 7b and 7c show simulated single-pulse social distancing strategies combined with a mild social distancing with $\beta_m = 0.3214$, and a periodic relaxation policy with the same weighted transmission rate average $\beta_m = 0.3214$ and small period time ($T = 1$ day and $r = 5/7$ is switching between the transmission rate of $\beta_n = 0.5$ and $\beta_d = 0.25$). This is consistent with the result in section 3.4, which states that fast switching policies (like Fig. 7c) converge to mild social distancing (like Fig. 7b) with weighted transmission rate averaged over time.

Figs. 7d and 7e show simulated single-pulse social distancing strategies combined with a periodic relaxation policy with $r = 5/7$ and period $T = 7$ one week, and $T = 14$ two weeks, respectively. The "V" shape pattern is still consistent for these combination policies, with similar approximated diagonal and vertical borders between the blue and white regions. Such policies are feasible to implement during an epidemic to allow some economic activities, and a *well-timed* additional single-pulse social distancing can significantly reduce the infected peak.

4 Conclusion and Discussion

The white area of the "V" shaped graphs shown in Figs. 2a and 5 represents a linear trade-off between the start time t_s and the duration t_d of social distancing, illustrated for several different epidemic models, some of which were recently proposed for COVID-19. A single interval social distancing would not be effective in reduction of the infected peak if the start time is too late (blue region on the right side of vertical line), or too early (the blue area on the bottom left side of the diagonal line). On the other hand, a single interval social distancing enacted at a *well-timed* can significantly reduce the infected peak.

For example Fig. 8 shows how a *well-timed* social distancing intervention can improve outcomes, for each of the investigated models. The dashed black line is the time-varying transmission rate $\beta(t)$, defined by (5),

bioRxiv preprint doi: https://doi.org/10.1101/2020.06.21.163931; this version posted June 22, 2020. The copyright holder for this preprint (which was not certified by peer review) is the author/funder. All rights reserved. No reuse allowed without permission.

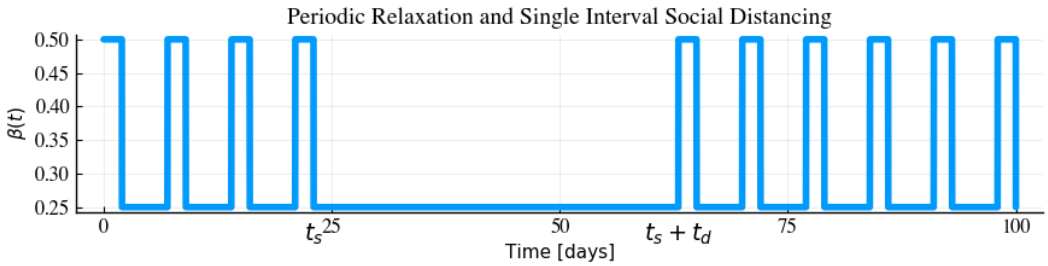

(a) Transmission rate $\beta(t)$ of periodic relaxation policy with period $T = 7$ and ratio of 5/7 to simulate five days social distancing relaxation policy per week, combined with a single-pulse social distancing from $t_s = 23$ for duration time of $t_d = 40$, that ends at time $t_s + t_d = 63$.

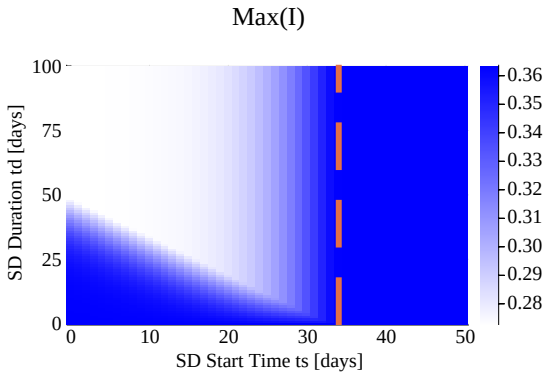

(b) Mild SD with $\beta_m = 0.3214$ combined with a single-pulse SD.

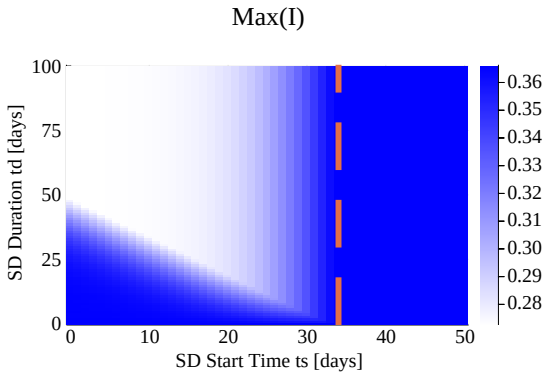

(c) Periodic SD with $T = 1$ and $r = 5/7$ combined with a single-pulse SD.

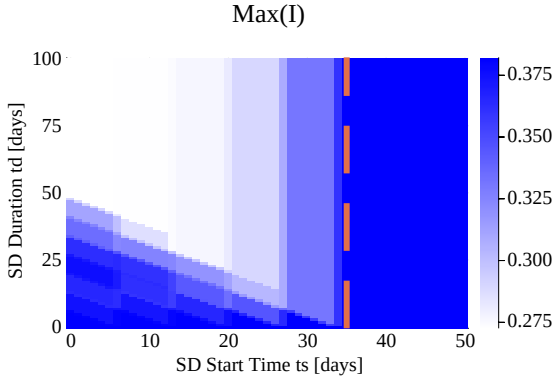

(d) Periodic relaxation with $T = 7$ and $r = 5/7$ combined with a single-pulse SD.

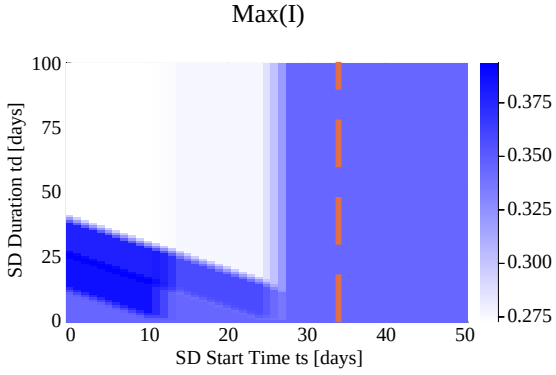

(e) Periodic relaxation with $T = 14$ and $r = 5/7$ combined with a single-pulse SD.

Figure 7: Effect of mild social distancing and periodic relaxation in combination with a single interval social distancing for *SIR* model.

switching between two values β_n and β_d. The black line represents the normalized infected compartment when using this input. The red and blue curves represent the infected compartment with $\beta(t) = \beta_n$, and $\beta(t) = \beta_d$ respectively. In other words, not having any social distancing enacted in a population (red curve), and starting social distancing at the beginning of an epidemic $t_s = 0$ for a long duration $t_d \to \infty$. It can be observed that the values of the peaks of the black and blue lines are close to each other. This indicates that a *proper* timing of single-pulse social distancing can have a significant impact on the infected peak in a way that the peak gets closer to the one that would occur in the case of a complete social distancing policy (blue line).

The ratio between transmission rates, β_n/β_d, is set to 2 for the simulations represented in Figs. 2, 5, 6, 7, and 8. This ratio is seen to be proportional to the slope of the diagonal border between the blue and white regions of Fig. 2 in Section 3.1. By increasing the transmission rate ratio β_n/β_d, i.e. having more restricted social distancing, the slope of the diagonal line will be higher. Fig. 9 shows the heat map of the normalized infected

bioRxiv preprint doi: https://doi.org/10.1101/2020.06.21.163931; this version posted June 22, 2020. The copyright holder for this preprint (which was not certified by peer review) is the author/funder. All rights reserved. No reuse allowed without permission.

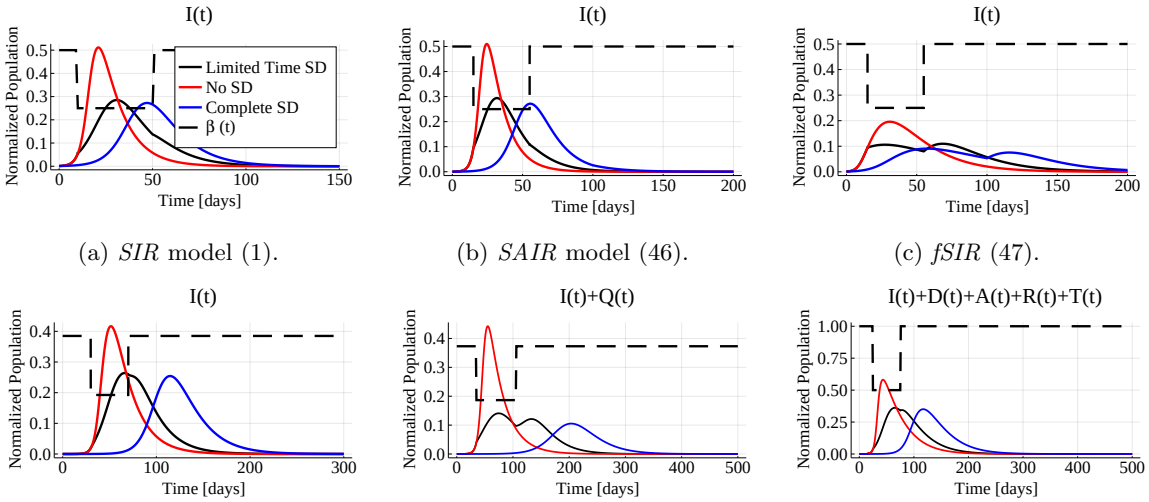

(a) *SIR* model (1). (b) *SAIR* model (46). (c) *fSIR* (47).

(d) 6 Compartment *SIR* model (48). (e) *SIQR* model (49). (f) *SIDARTHE* model (50).

Figure 8: Optimal social distancing and quarantine period during an epidemic based on different models: a) The *SIR* model (1), b) the *SAIR* model presented in Appendix C.1, c) the six-compartment *SIR* model with social distancing from [26] presented in Appendix C.3, d) the *fSIR* [46] presented in Appendix C.2, e) the *SIQR* model [37] presented in Appendix C.4, and f) and the *SIDARTHE* model [36] presented in Appendix C.5. Dashed line shows the input $\beta(t)$ applied in each model as a social distancing control. The black line represents the infected compartment with limited time social distancing, the red line shows the dynamics of the infected compartment with $\beta(t) = \beta_n$ (no social distancing), and the blue line represents the scenario of having the social distancing during an entire epidemic with $\beta(t) = \beta_d$.

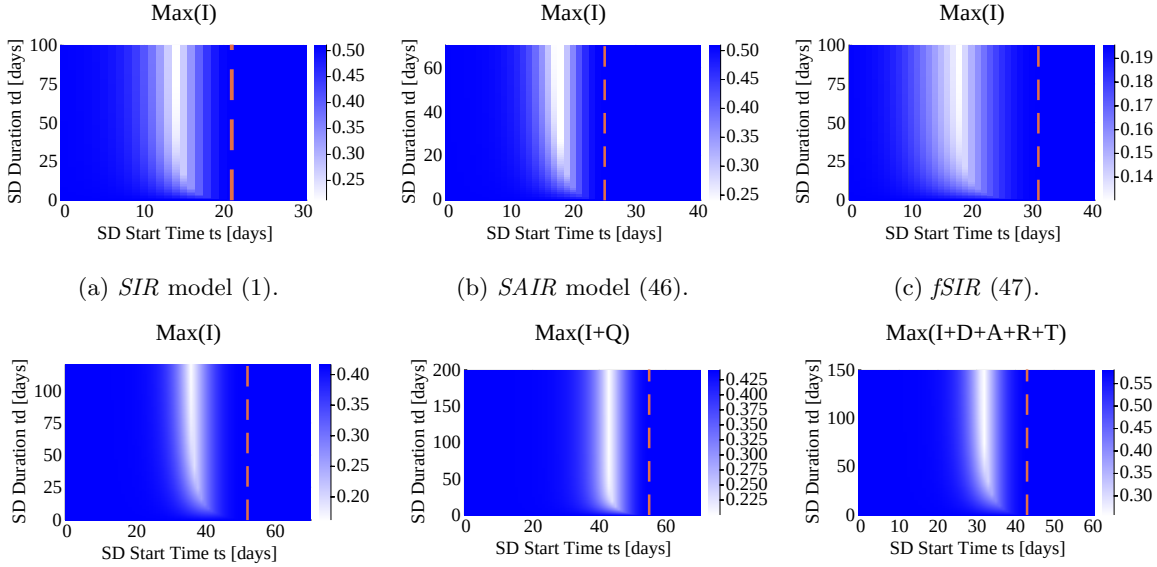

(a) *SIR* model (1). (b) *SAIR* model (46). (c) *fSIR* (47).

(d) 6 Compartment *SIR* model (48). (e) *SIQR* model (49). (f) *SIDARTHE* model (50).

Figure 9: Maximum of the infected compartment for the some of the recent models introduced to capture the COVID-19 behavior. Models and their parameters are fully presented in Appendix C. The ratio between transmission rates in the single-pulse strategy is $\beta_n/\beta_d = 10$.

peak of the investigated models when, instead, $\beta_n/\beta_d = 10$. Note, the β_n is the same for the investigated models in Figs. 5, 9. It can be observed that social distancing pulses that take place at an early time of an epidemic will not be effective in diminishing the peak of the infected population. Intuitively, the blue area on the left side of vertical white region is for the scenarios when the infected peak occurs after the social distancing time interval. But, if a social distancing is imposed from the white region based on the suggested start time t_s and duration t_d of social distancing, then it will be most effective in lowering the infected peak.

To sum up, we have introduced a trade-off between the start time and the duration of social distancing effects

bioRxiv preprint doi: https://doi.org/10.1101/2020.06.21.163931; this version posted June 22, 2020. The copyright holder for this preprint (which was not certified by peer review) is the author/funder. All rights reserved. No reuse allowed without permission.

on the peak of the infected population. A "V" shape pattern has been observed for the *SIR* model. This pattern can be understood mathematically in the special case of the *SIR* model, and is verfied through simulation for more complex models recently proposed for COVID-19. A single pulse of social distancing is shown to be most effective if it happens at a *proper time*. Moreover, the infected peak for economically preferable strategies like mild social distancing or periodic social distancing relaxation can be reduced by a single pulse of social distancing.

Computational Resources

The numerical simulations and plots are done with the DifferentialEquations package [70] of Julia programming language [71], and the analysis notebook are available on `https://github.com/sontaglab/epidemics` repository.

Acknowledgments

The Authors thank M. Ali Al-Radhawi for his comments.

Appendix A *SIR* Model

A.1 Peak of the infected compartment

The peak of the infected compartment for the simple *SIR* model can be characterized at the time when $\dot{I}(t) = 0$, from Eq. (1b). This is the time when the rates at which populations are being infected and recovered (or removed) from the infected compartment balance out. The normalized susceptible population at the peak of infected compartment is $S_p = \gamma/\beta$, which can be re-written in terms of the basic reproduction number $R_0 = \beta/\gamma$, as $S_p = R_0^{-1}$. Furthermore, the value of the infected compartment can be obtained by the following derived implicit formula between the susceptible S, and infected I compartments:

$$\dot{I} = -\dot{S} + R_0^{-1}\left(\frac{\dot{S}}{S}\right) \tag{35}$$

$$\to I - I(0) = -(S - S(0)) + R_0^{-1} \ln \frac{S}{S(0)}, \tag{36}$$

Here $S(0)$ and $I(0)$ are the initial values of the susceptible and infected compartments at the beginning of the epidemic. Therefore, the peak of the infected compartment is:

$$I_p = I(0) + S(0) - S_p + R_0^{-1} \ln \frac{S_p}{S(0)} \tag{37a}$$

$$= I(0) + S(0) - R_0^{-1}\left(1 + \ln\left(R_0 S(0)\right)\right). \tag{37b}$$

If we assume that $S(0) \approx 1$, and $I(0) \approx 0$ then the infected peak will be simplified to:

$$I_p \approx 1 - R_0^{-1}\left(1 + \ln\left(R_0\right)\right). \tag{38}$$

A.2 Change of variables for *SIR* model

To gain a better understanding of the infected compartment peak time t_p, we can reparametrize the time t by τ in the form of $\mathrm{d}\tau/\,\mathrm{d}t = I(t)$ with initial time $t_0 = \tau_0 = 0$ as suggested by [72], the *SIR* model(1), under this change of time scale, is now linear:

$$\frac{\mathrm{d}S}{\mathrm{d}\tau} = -\beta S, \tag{39a}$$

$$\frac{\mathrm{d}I}{\mathrm{d}\tau} = \beta S - \gamma, \tag{39b}$$

$$\frac{\mathrm{d}R}{\mathrm{d}\tau} = \gamma. \tag{39c}$$

We remark that his transformed system evolves from $\tau = 0$ to $\tau = \int_0^\infty I(s)\,\mathrm{d}s < \infty$. The solution of the linearized model can be written in the following form

$$S = S(0)\exp(-\beta\tau), \tag{40a}$$

$$I = I(0) + S(0) - S(0)\exp(-\beta\tau) - \gamma\tau, \tag{40b}$$

$$R = R(0) + \gamma\tau, \tag{40c}$$

$$t = \int_0^\tau \frac{\mathrm{d}\tau'}{I(0) + S(0) - S(0)\exp(-\beta\tau') - \gamma\tau'}. \tag{40d}$$

bioRxiv preprint doi: https://doi.org/10.1101/2020.06.21.163931; this version posted June 22, 2020. The copyright holder for this preprint (which was not certified by peer review) is the author/funder. All rights reserved. No reuse allowed without permission.

The infected peak and its corresponding time can be written analytically as follows:

$$S_p = \gamma/\beta = R_0^{-1}, \tag{41a}$$
$$\tau_p = \ln(R_0 S(0))/\beta, \tag{41b}$$
$$I_p = I(0) + S(0) - R_0^{-1}(1 + \ln(R_0 S(0))), \tag{41c}$$
$$t_p = \int_0^{\tau_p} \frac{\mathrm{d}\tau'}{I(0) + S(0) - \exp(-\beta\tau') - \gamma\tau'}. \tag{41d}$$

It can be observed that the maximum of the infected compartment is only a function of the basic reproduction number R_0, while the time of the peak τ_p is dependent on R_0 and β.

Also, a different time scaling and shifting have been used by [73] to show statistical similarities of the COVID-19 spread in different countries.

A.3 Linear approximation

To gain a better understanding of $I(t)$, here we have to deal with the integral represented in (40d). To avoid the complexity and have an intuitive approximation for small times for $I(t)$ from equation (39b), we'll consider $S(t)$ to be constant, and therefore equal to its initial value $S(0)$. That gives:

$$\dot{I} \approx (\beta S(0) - \gamma) I, \tag{42a}$$
$$\rightarrow I(t) \approx I(0) \exp((\beta S(0) - \gamma)t), \tag{42b}$$
$$\approx I(0) \exp((\beta - \gamma)t). \tag{42c}$$

This approximation is reasonable for the beginning of the spread of the virus, when $S(t)$ is close to one, the total population. We used this approximation in section 3.1.

Appendix B Fast Switching Policies

Consider a general system affine in controls ([74]):

$$\dot{x}(t) = f_0[x(t)] + \sum_{i=1}^{m} \beta_i(t) f_i[x(t)]. \tag{43}$$

Let us suppose that the inputs $\beta_i(t)$ are periodic with period T, and consider the constant control obtained by averaging the β_i over a period:

$$\bar{\beta}_i := \frac{1}{T} \int_0^T \beta_i(t)\, \mathrm{d}t. \tag{44}$$

It can be proved that, if the frequency of $\beta(t) = (\beta_1(t), \ldots, \beta_m(t))$ goes to infinity, meaning that the switching time approaches 0, then solutions approach those for the average $\bar{\beta}$. This follows from standard averaging results for systems that are affine in controls. Specifically, (1) the map from controls on an interval $[0, T]$ to trajectories on $[0, T]$ is continuous with respect to the weak* topology in L^1 and the uniform topology on continuous functions, respectively (see, e.g. [74], Theorem 1), and (2) for a periodic input $u(t)$, the input $u(\omega t)$ converges weakly to the average of u as $\omega \to \infty$. An alternative proof is given for example in the textbook [75] (section 10.2) (changing time scale in the statement of Theorem 10.4, by $x(t) = x(t/\epsilon)$). (This fact was also observed in [64].)

Appendix C State Space Representation of Epidemic Models

We describe several; epidemic models that have recently proposed for COVID-19, we use the state space formulation (43). For example, the *SIR* model represented in (1) can expressed, using the state $x = (S, I, R)$, in the following form:

$$f_0(x) = \begin{pmatrix} 0 \\ -\gamma x_2 \\ \gamma x_2 \end{pmatrix}, \quad f_1(x) = \begin{pmatrix} -x_1 x_2 \\ x_1 x_2 \\ 0 \end{pmatrix}. \tag{45}$$

We used in all simulations the parameters $(\beta, \gamma) = [0.5, 0.09]$ with initial conditions of $(S, I, R)_{t=0} = (1 - 10^{-3}, 10^{-3}, 0)$. The value of $\beta(t)$ used for the social distancing intervals of Fig. 2 and Fig. 9a are 0.25, and 0.05 respectively.

bioRxiv preprint doi: https://doi.org/10.1101/2020.06.21.163931; this version posted June 22, 2020. The copyright holder for this preprint (which was not certified by peer review) is the author/funder. All rights reserved. No reuse allowed without permission.

C.1 *SAIR* model

The *SAIR* model as a simple extension of the *SIR* model with an asymptomatic A compartment in the population. The state space representation in terms of the state $x = (S, A, I, R)$ is:

$$f_0(x) = \begin{pmatrix} 0 \\ -(\nu+\alpha)x_2 \\ \nu x_2 - \gamma x_3 \\ \alpha x_4 + \gamma x_3 \end{pmatrix}, \quad f_1(x) = \begin{pmatrix} -x_1 x_2 \\ x_1 x_2 \\ 0 \\ 0 \end{pmatrix}, \quad f_2(x) = \begin{pmatrix} -x_1 x_3 \\ 0 \\ x_1 x_3 \\ 0 \end{pmatrix}. \tag{46}$$

We use the parameters $(\beta_1, \beta_2, \nu, \alpha, \gamma) = [0.3, 0.5, 0.1, 0.5, 0.09]$ with initial conditions of $(S, A, I, R)_{t=0} = (1 - 1.1 \times 10^{-3}, 10^{-3}, 10^{-4}, 0)$. The values of $\beta_1(t)$ and $\beta_2(t)$ used for the social distancing intervals of Fig. 5a and Fig. 9b are half ($\beta_n/\beta_d = 2$), and 10% ($\beta_n/\beta_d = 10$) of their original value respectively.

C.2 *fSIR* model

An"infection aware" distancing model has been recently introduced by [46], in order to account for how individuals practice enhanced social distancing as the number of infections increases. This model has an additional term of the form $1/(1 + kI)$ in comparison with the simple *SIR* model (1) where k is the feedback gain of the statistical social awareness effect on disease spread. The state variable is $x = (S, I, R)$ and the state space representation is as follows:

$$f_0(x) = \begin{pmatrix} 0 \\ -\gamma x_2 \\ \gamma x_2 \end{pmatrix}, \quad f_1(x) = \begin{pmatrix} -x_1 x_2/(1+kx_2) \\ x_1 x_2/(1+kx_2) \\ 0 \end{pmatrix}. \tag{47}$$

We use the parameters $(\beta, \gamma, k) = [0.5, 0.09, 10]$ with initial conditions are $(S, I, R)_{t=0} = (1 - 10^{-3}, 10^{-3}, 0)$. The values of $\beta(t)$ used for the social distancing intervals of Fig. 5b and Fig. 9c are 0.25, and 0.05 respectively.

C.3 Six-compartment *SIR* model

The 6 compartment *SIR* model [26] with state variable $x = (S_D, S_N, A_D, A_N, I_D, I_N, R)$ is:

$$f_0(x) = \begin{pmatrix} -h_1 x_1 + h_2 x_2 \\ h_1 x_1 - h_2 x_2 \\ -\gamma_{AI} x_3 + h_2 x_4 - h_1 x_3 \\ -\gamma_{AI} x_4 - h_2 x_4 + h_1 x_3 \\ f\gamma_{AI}(x_3 + x_4) - \delta x_5 - \gamma_{IR} x_5 \\ (1-f)\gamma_{AI}(x_3 + x_4) + \gamma_{IR} x_5 \end{pmatrix}, f_1(x) = \begin{pmatrix} -\epsilon_S x_1 x_5 \\ -x_2 x_5 \\ \epsilon_S x_1 x_5 \\ x_2 x_5 \\ 0 \\ 0 \end{pmatrix}, f_2(x) = \begin{pmatrix} -\epsilon_S(x_4 + \epsilon_A x_3)x_1 \\ -(x_4 + \epsilon_A x_3)x_2 \\ \epsilon_S(x_4 + \epsilon_A x_3)x_1 \\ (x_4 + \epsilon_A x_3)x_2 \\ 0 \\ 0 \end{pmatrix}. \tag{48}$$

We use the parameters $(\beta_A, \epsilon_A, \epsilon_S, \beta_I, \gamma_{AI}, \gamma_{AR}, f, \delta) = [0.385, 0.32, 0.32, 0.2464, 0, 0.196, 0.048, 0.821, 2.4e-3, 30, 40]$ and initial conditions $(S_D, S_N, A_D, A_N, I_D, I_N, R)_{t=0} = (0, 1 - 10^{-5}, 0, 0, 10^{-5}, 0)$, as suggested by the authors. The values of $\beta_1(t) = \beta_A(t)$ and $\beta_2(t) = \beta_I(2)$ used for the social distancing intervals of Fig. 5c and Fig. 9d are half ($\beta_n/\beta_d = 2$), and 10% ($\beta_n/\beta_d = 10$) of their original value respectively.

C.4 *SIQR* model

The *SIQR* model [37, 64] with state variable $x = (S, I, Q, R)$ is:

$$f_0(x) = \begin{pmatrix} 0 \\ -(\alpha+\eta)x_2 \\ -\delta x_3 + \eta x_2 \\ \alpha x_2 \end{pmatrix}, \quad f_1(x) = \begin{pmatrix} -x_1 x_2 \\ x_1 x_2 \\ 0 \\ 0 \end{pmatrix}. \tag{49}$$

We use the parameters $(\beta, \alpha, \eta, \delta, N) = [0.373, 0.067, 0.067, 0.036, 10^7]$ with initial conditions are $(S, I, R)_{t=0} = (10^7 - 83.333, 83.333, 0, 0)$, as suggested by the authors. The value of $\beta(t) = q\beta$ used for the social distancing intervals of Fig. 5d and Fig. 9e is half ($\beta_n/\beta_d = 2$), and 10% ($\beta_n/\beta_d = 10$) of their original value respectively.

bioRxiv preprint doi: https://doi.org/10.1101/2020.06.21.163931; this version posted June 22, 2020. The copyright holder for this preprint (which was not certified by peer review) is the author/funder. All rights reserved. No reuse allowed without permission.

C.5 *SIDARTHE* model

The *SIDARTHE* model [36, 64] with state variable $x = (S, I, D, A, R, T, H, E)$ is:

$$f_0(x) = \begin{pmatrix} 0 \\ -(p_5 + p_6 + p_7)x_2 \\ p_5x_2 - (p_8 + p_9)x_3 \\ p_6x_2 - (p_{10} + p_{11} + p_{12})x_4 \\ p_8x_3 + p_{10}x_4 - (p_{13} + p_{14})x_5 \\ p_{11}x_4 + p_{13}x_5 - (p_{13} + p_{14})x_6 \\ p_7x_2 + p_9x_3 + p_{12}x_4 + p_{14}x_5 + p_15x_6 \\ p_{16}x_6 \end{pmatrix}, \quad f_1(x) = \begin{pmatrix} -x_1x_2 \\ x_1x_2 \\ 0 \\ 0 \\ 0 \\ 0 \\ 0 \\ 0 \end{pmatrix}. \tag{50}$$

The parameters are $N = 10^7$ and the p_i are shown below. Initial conditions are $(S, I, D, A, R, T, H, E)_{t=0} = (10^7 - 83.333, 83.333, 0, 0, 0, 0, 0, 0)$, as suggested by the authors. The value of $\beta(t) = q\beta$ used for the social distancing intervals of Fig. 5d and Fig. 9e are half ($\beta_n/\beta_d = 2$), and 10% ($\beta_n/\beta_d = 10$) of their original value respectively. The parameters p_i are the entries of the following vector p:

$$p = [0.570, 0.011, 0.456, 0.011, 0.171, 0.371, 0.125, 0.125, 0.012, 0.027, 0.003, 0.034, 0.034, 0.017, 0.017, 0.017]$$

bioRxiv preprint doi: https://doi.org/10.1101/2020.06.21.163931; this version posted June 22, 2020. The copyright holder for this preprint (which was not certified by peer review) is the author/funder. All rights reserved. No reuse allowed without permission.

References

[1] W. H. Organization *et al.*, "Coronavirus disease 2019 (covid-19): situation report, 72," 2020.

[2] C. Map, "Tracking the global outbreak," *The New York Times, Updated on March*, vol. 18, 2020.

[3] A. L. Wright, K. Sonin, J. Driscoll, and J. Wilson, "Poverty and economic dislocation reduce compliance with covid-19 shelter-in-place protocols," *University of Chicago, Becker Friedman Institute for Economics Working Paper*, no. 2020-40, 2020.

[4] A. Sarin and A. Sarin, "Coronavirus disease (covid-19): Spread, awareness and strategic containment," *Journal of Communicable Diseases (E-ISSN: 2581-351X & P-ISSN: 0019-5138)*, vol. 52, no. 1, pp. 22–31, 2020.

[5] M. S. Wolf, M. Serper, L. Opsasnick, R. M. O'Conor, L. M. Curtis, J. Y. Benavente, G. Wismer, S. Batio, M. Eifler, P. Zheng *et al.*, "Awareness, attitudes, and actions related to covid-19 among adults with chronic conditions at the onset of the us outbreak: a cross-sectional survey," *Annals of Internal Medicine*, 2020.

[6] S. Gupta, T. D. Nguyen, F. L. Rojas, S. Raman, B. Lee, A. Bento, K. I. Simon, and C. Wing, "Tracking public and private response to the covid-19 epidemic: Evidence from state and local government actions," National Bureau of Economic Research, Tech. Rep., 2020.

[7] G. Scally, B. Jacobson, and K. Abbasi, "The uk's public health response to covid-19," 2020.

[8] V. Gritsenko, O. Skugarevsky, V. Konstantinov, N. Khamenka, T. Marinova, A. Reznik, and R. Isralowitz, "Covid 19 fear, stress, anxiety, and substance use among russian and belarusian university students."

[9] M. Dahlberg, P.-A. Edin, E. Grönqvist, J. Lyhagen, J. Östh, A. Siretskiy, and M. Toger, "Effects of the covid-19 pandemic on population mobility under mild policies: Causal evidence from sweden," *arXiv preprint arXiv:2004.09087*, 2020.

[10] L. Hensvik and O. Skans, "Covid-19 crisis response monitoring: Sweden," 2020.

[11] Y. Berman, "The distributional short-term impact of the covid-19 crisis on wages in the united states," *arXiv preprint arXiv:2005.08763*, 2020.

[12] C. Courtemanche, J. Garuccio, A. Le, J. Pinkston, and A. Yelowitz, "Strong social distancing measures in the united states reduced the covid-19 growth rate: Study evaluates the impact of social distancing measures on the growth rate of confirmed covid-19 cases across the united states." *Health Affairs*, pp. 10–1377, 2020.

[13] W. F. Maloney and T. Taskin, "Determinants of social distancing and economic activity during covid-19: A global view," *World Bank Policy Research Working Paper*, no. 9242, 2020.

[14] G. Albi, L. Pareschi, and M. Zanella, "Relaxing lockdown measures in epidemic outbreaks using selective socio-economic containment with uncertainty," *medRxiv*, 2020.

[15] F. Piguillem and L. Shi, "Optimal covid-19 quarantine and testing policies," 2020.

[16] F. E. Alvarez, D. Argente, and F. Lippi, "A simple planning problem for covid-19 lockdown," National Bureau of Economic Research, Tech. Rep., 2020.

[17] H. Ito, "Input-to-state stability and lyapunov functions with explicit domains for sir model of infectious diseases," *arXiv preprint arXiv:2005.13378*, 2020.

[18] C. Tian, Q. Zhang, and L. Zhang, "Global stability in a networked sir epidemic model," *Applied Mathematics Letters*, p. 106444, 2020.

[19] F. Liu, S. Cui, X. Li, and M. Buss, "On the stability of the endemic equilibrium of a discrete-time networked epidemic model," *arXiv preprint arXiv:2001.07451*, 2020.

[20] Y. Liu, L. Ding, X. An, P. Hu, and F. Du, "Epidemic spreading on midscopic multi-layer network with optimal control mechanism," *Physica A: Statistical Mechanics and its Applications*, vol. 537, p. 122775, 2020.

[21] G. Stewart, K. Heusden, and G. A. Dumont, "How control theory can help us control covid-19," *IEEE Spectrum*, vol. 57, no. 6, pp. 22–29, 2020.

[22] A. Goodman-Bacon and J. Marcus, "Using difference-in-differences to identify causal effects of covid-19 policies," 2020.

[23] W. O. Kermack and A. G. McKendrick, "A contribution to the mathematical theory of epidemics," *Proceedings of the royal society of london. Series A, Containing papers of a mathematical and physical character*, vol. 115, no. 772, pp. 700–721, 1927.

[24] F. Brauer, C. Castillo-Chavez, and Z. Feng, *Mathematical Models in Epidemiology*. Springer, 2019.

[25] G. Albi, L. Pareschi, and M. Zanella, "Control with uncertain data of socially structured compartmental epidemic models," *arXiv preprint arXiv:2004.13067*, 2020.

bioRxiv preprint doi: https://doi.org/10.1101/2020.06.21.163931; this version posted June 22, 2020. The copyright holder for this preprint (which was not certified by peer review) is the author/funder. All rights reserved. No reuse allowed without permission.

[26] J. Gevertz, J. Greene, C. Hixahuary Sanchez Tapia, and E. D. Sontag, "A novel covid-19 epidemiological model with explicit susceptible and asymptomatic isolation compartments reveals unexpected consequences of timing social distancing," *medRxiv*, 2020. [Online]. Available: https://www.medrxiv.org/content/early/2020/05/18/2020.05.11.20098335

[27] W. Pang, "Public health policy: Covid-19 epidemic and seir model with asymptomatic viral carriers," *arXiv preprint arXiv:2004.06311*, 2020.

[28] A. Etxeberria-Iriondo, M. De la Sen, and S. Alonso-Quesada, "A new epidemic model under vaccination," in *2019 14th IEEE Conference on Industrial Electronics and Applications (ICIEA)*. IEEE, 2019, pp. 2388–2392.

[29] T. Sun and D. Weng, "Estimating the effects of asymptomatic and imported patients on covid-19 epidemic using mathematical modeling," *Journal of Medical Virology*, 2020.

[30] G. Gaeta, "Asymptomatic infectives and r_0 for covid," *arXiv preprint arXiv:2003.14098*, 2020.

[31] Z. Liu, P. Magal, O. Seydi, and G. Webb, "A covid-19 epidemic model with latency period," *Infectious Disease Modelling*, 2020.

[32] J. B. Aguilar, J. S. Faust, L. M. Westafer, and J. B. Gutierrez, "Investigating the impact of asymptomatic carriers on covid-19 transmission," *medRxiv*, 2020.

[33] U. A.-P. de León, A. G. Pérez, and E. Avila-Vales, "A data driven analysis and forecast of an seiard epidemic model for covid-19 in mexico," *arXiv preprint arXiv:2004.08288*, 2020.

[34] I. Korolev, "Identification and estimation of the seird epidemic model for covid-19," Working paper, Tech. Rep., 2020.

[35] C. Reno, J. Lenzi, A. Navarra, E. Barelli, D. Gori, A. Lanza, R. Valentini, B. Tang, and M. P. Fantini, "Forecasting covid-19-associated hospitalizations under different levels of social distancing in lombardy and emilia-romagna, northern italy: Results from an extended seir compartmental model," *Journal of Clinical Medicine*, vol. 9, no. 5, p. 1492, 2020.

[36] G. Giordano, F. Blanchini, R. Bruno, P. Colaneri, A. Di Filippo, A. Di Matteo, M. Colaneri *et al.*, "A sidarthe model of covid-19 epidemic in italy," *arXiv preprint arXiv:2003.09861*, 2020.

[37] M. G. Pedersen and M. Meneghini, "Quantifying undetected covid-19 cases and effects of containment measures in italy," *ResearchGate Preprint (online 21 March 2020) DOI*, vol. 10, 2020.

[38] S. Mandal, T. Bhatnagar, N. Arinaminpathy, A. Agarwal, A. Chowdhury, M. Murhekar, R. R. Gangakhedkar, and S. Sarkar, "Prudent public health intervention strategies to control the coronavirus disease 2019 transmission in india: A mathematical model-based approach," *The Indian journal of medical research*, vol. 151, no. 2-3, p. 190, 2020.

[39] X. Bardina, M. Ferrante, and C. Rovira, "A stochastic epidemic model of covid-19 disease," *arXiv preprint arXiv:2005.02859*, 2020.

[40] Y. Bai, L. Yao, T. Wei, F. Tian, D.-Y. Jin, L. Chen, and M. Wang, "Presumed asymptomatic carrier transmission of covid-19," *Jama*, vol. 323, no. 14, pp. 1406–1407, 2020.

[41] N. Aguirre-Duarte, "Can people with asymptomatic or pre-symptomatic covid-19 infect others: a systematic review of primary data," *medRxiv*, 2020.

[42] X. Yu and R. Yang, "Covid-19 transmission through asymptomatic carriers is a challenge to containment," *Influenza and Other Respiratory Viruses*, 2020.

[43] Z. Hu, C. Song, C. Xu, G. Jin, Y. Chen, X. Xu, H. Ma, W. Chen, Y. Lin, Y. Zheng *et al.*, "Clinical characteristics of 24 asymptomatic infections with covid-19 screened among close contacts in nanjing, china," *Science China Life Sciences*, pp. 1–6, 2020.

[44] K. A. Kabir, K. Kuga, and J. Tanimoto, "Analysis of sir epidemic model with information spreading of awareness," *Chaos, Solitons & Fractals*, vol. 119, pp. 118–125, 2019.

[45] T. C. Reluga, "Game theory of social distancing in response to an epidemic," *PLoS computational biology*, vol. 6, no. 5, 2010.

[46] E. Franco, "A feedback sir (fsir) model highlights advantages and limitations of infection-based social distancing," *arXiv preprint arXiv:2004.13216*, 2020.

[47] N. Ghaffarzadegan and H. Rahmandad, "Simulation-based estimation of the spread of covid-19 in iran," *medRxiv*, 2020.

[48] S. Hsiang, D. Allen, S. Annan-Phan, K. Bell, I. Bolliger, T. Chong, H. Druckenmiller, A. Hultgren, L. Y. Huang, E. Krasovich *et al.*, "The effect of large-scale anti-contagion policies on the coronavirus (covid-19) pandemic," *MedRxiv*, 2020.

[49] M. Chinazzi, J. T. Davis, M. Ajelli, C. Gioannini, M. Litvinova, S. Merler, A. P. y Piontti, K. Mu, L. Rossi, K. Sun *et al.*, "The effect of travel restrictions on the spread of the 2019 novel coronavirus (covid-19) outbreak," *Science*, vol. 368, no. 6489, pp. 395–400, 2020.

bioRxiv preprint doi: https://doi.org/10.1101/2020.06.21.163931; this version posted June 22, 2020. The copyright holder for this preprint (which was not certified by peer review) is the author/funder. All rights reserved. No reuse allowed without permission.

[50] S. Flaxman, S. Mishra, A. Gandy, H. J. T. Unwin, T. A. Mellan, H. Coupland, C. Whittaker, H. Zhu, T. Berah, J. W. Eaton *et al.*, "Estimating the effects of non-pharmaceutical interventions on covid-19 in europe," *Nature*, pp. 1–8, 2020.

[51] X.-F. San, Z.-C. Wang, and Z. Feng, "Spreading speed and traveling waves for an epidemic model in a periodic patchy environment," *Communications in Nonlinear Science and Numerical Simulation*, p. 105387, 2020.

[52] F. Di Lauro, I. Z. Kiss, and J. Miller, "The timing of one-shot interventions for epidemic control," *medRxiv*, 2020.

[53] H. Khadilkar, T. Ganu, and D. P. Seetharam, "Optimising lockdown policies for epidemic control using reinforcement learning," *arXiv preprint arXiv:2003.14093*, 2020.

[54] M. U. Kraemer, C.-H. Yang, B. Gutierrez, C.-H. Wu, B. Klein, D. M. Pigott, L. Du Plessis, N. R. Faria, R. Li, W. P. Hanage *et al.*, "The effect of human mobility and control measures on the covid-19 epidemic in china," *Science*, vol. 368, no. 6490, pp. 493–497, 2020.

[55] M. Gatto, E. Bertuzzo, L. Mari, S. Miccoli, L. Carraro, R. Casagrandi, and A. Rinaldo, "Spread and dynamics of the covid-19 epidemic in italy: Effects of emergency containment measures," *Proceedings of the National Academy of Sciences*, vol. 117, no. 19, pp. 10 484–10 491, 2020.

[56] P. Coletti, P. Libin, O. Petrof, S. Abrams, C. Faes, P. Beutels, and N. Hens, "Covid-19 report on a meta-population model for belgium: a first status report," 2020.

[57] B. S. Pujari and S. M. Shekatkar, "Multi-city modeling of epidemics using spatial networks: Application to 2019-ncov (covid-19) coronavirus in india," *medRxiv*, 2020.

[58] B. Banerjee, P. K. Pandey, and B. Adhikari, "A model for the spread of an epidemic from local to global: A case study of covid-19 in india," *arXiv preprint arXiv:2006.06404*, 2020.

[59] C. Arellano, Y. Bai, G. Mihalache *et al.*, "Deadly debt crises: Covid-19 in emerging markets," Tech. Rep., 2020.

[60] O. Coibion, Y. Gorodnichenko, and M. Weber, "The cost of the covid-19 crisis: Lockdowns, macroeconomic expectations, and consumer spending," National Bureau of Economic Research, Tech. Rep., 2020.

[61] C. Garriga, R. Manuelli, S. Sanghi *et al.*, "Optimal management of an epidemic: Lockdown, vaccine and value of life," Tech. Rep., 2020.

[62] T. Andersson, A. Erlanson, D. Spiro, and R. Östling, "Optimal trade-off between economic activity and health during an epidemic," *arXiv preprint arXiv:2005.07590*, 2020.

[63] J. C. Miller and Y. Ge, "If long-term suppression is not possible, how do we minimize mortality for covid-19 and other emerging infectious disease outbreaks?"

[64] M. Bin, P. Cheung, E. Crisostomi, P. Ferraro, C. Myant, T. Parisini, and R. Shorten, "On fast multi-shot epidemic interventions for post lock-down mitigation: Implications for simple covid-19 models," *arXiv preprint arXiv:2003.09930*, 2020.

[65] A. Zargar, "Lockdown measures eased even as india becomes asia's covid hub," https://www.cbsnews.com/news/coronavirus-in-india-lockdown-measures-ease-as-covid-infections-mount-today-2020-05-19/, May 2020.

[66] T. Lancet, "India under covid-19 lockdown," *Lancet (London, England)*, vol. 395, no. 10233, p. 1315, 2020.

[67] D. Kai, G.-P. Goldstein, A. Morgunov, V. Nangalia, and A. Rotkirch, "Universal masking is urgent in the covid-19 pandemic: Seir and agent based models, empirical validation, policy recommendations," *arXiv preprint arXiv:2004.13553*, 2020.

[68] T. Kruse and P. Strack, "Optimal control of an epidemic through social distancing," 2020.

[69] O. Karin, Y. M. Bar-On, T. Milo, I. Katzir, A. Mayo, Y. Korem, B. Dudovich, E. Yashiv, A. J. Zehavi, N. Davidovitch *et al.*, "Cyclic exit strategies to suppress covid-19 and allow economic activity."

[70] C. Rackauckas and Q. Nie, "Differentialequations. jl–a performant and feature-rich ecosystem for solving differential equations in julia," *Journal of Open Research Software*, vol. 5, no. 1, 2017.

[71] J. Bezanson, A. Edelman, S. Karpinski, and V. B. Shah, "Julia: A fresh approach to numerical computing," *SIAM Review*, vol. 59, no. 1, pp. 65–98, 2017. [Online]. Available: https://doi.org/10.1137/141000671

[72] M. Cadoni, "How to reduce epidemic peaks keeping under control the time-span of the epidemic," *arXiv preprint arXiv:2004.02189*, 2020.

[73] A. S. Kim, "Transformed time series analysis of first-wave covid-19: universal similarities found in the group of twenty (g20) countries," *medRxiv*, 2020. [Online]. Available: https://www.medrxiv.org/content/early/2020/06/14/2020.06.11.20128991

[74] E. D. Sontag, *Mathematical control theory: deterministic finite dimensional systems*. Springer Science & Business Media, 2013, vol. 6.

[75] H. K. Khalil and J. W. Grizzle, *Nonlinear systems*. Prentice hall Upper Saddle River, NJ, 2002, vol. 3.